



## CFD Based Numerical Performance Assessment of a Solar Air Heater Duct Roughened by Transverse - Trapezoidal Sectioned Ribs

Kadhim K. Idan Al-Chlahawi<sup>1\*</sup>, Bahjat Hassan Alyas<sup>2</sup>, Abdullah A. Badr<sup>2</sup>

<sup>1</sup> Department of Mechanical Engineering, University of Al-Qadisiyah, Al-Qadisiyah 58001, Iraq

<sup>2</sup> Technical Engineering College, Northern Technical University, Mosul 41003, Iraq

Corresponding Author Email: [kadhim.idan@qu.edu.iq](mailto:kadhim.idan@qu.edu.iq)

<https://doi.org/10.18280/ijht.410517>

### ABSTRACT

**Received:** 10 July 2023

**Revised:** 6 October 2023

**Accepted:** 11 October 2023

**Available online:** 31 October 2023

#### Keywords:

*solar air heater, artificial roughness, numerical simulation, turbulence modeling, heat transfer enhancement, RNG k-ε model*

The convective heat transfer coefficient in solar air heaters suffers from a reduction due to the formation of a laminar sub-layer between the absorber plate and the air in motion. A viable and efficient strategy to augment the heat transfer coefficient involves introducing artificial roughness in the form of ribs. This study employs numerical simulations to examine the turbulent heat and flow characteristics within a rectangular duct of a solar air heater (SAH) featuring trapezoidal ribs as roughness elements. The governing equations were numerically solved using the finite-volume method and ANSYS FLUENT. The transport equations of turbulent kinetic energy and its dissipation rate were addressed by the RNG  $k-\epsilon$  turbulence model. The Nusselt number ( $Nu$ ), friction factor ( $f$ ), and thermal performance factor (TPF) were computed across a broad range of conditions, including Reynolds number ( $6,000 \leq Re \leq 18,000$ ), relative roughness height ( $0.021 \leq e/D_h \leq 0.043$ ), and relative roughness pitch ( $5 \leq P/e \leq 20$ ) under constant heat flux conditions. It was determined that the maximum enhancement ratio of  $Nu$  was 2.124 times that of a smooth duct when  $e/D_h=0.043$ ,  $P/e=20$ , and  $Re=6,000$ . Additionally, the TPF for the SAH featuring trapezoidal ribs attained a peak value of 1.64.

## 1. INTRODUCTION

Solar air heaters (SAHs) have emerged as pivotal instruments for harnessing renewable energy, offering significant utility for space heating and industrial applications. The primary operation of a SAH involves solar energy absorption by an absorber plate, which is subsequently transmitted to the flowing air. However, due to the emergence of a laminar sub-layer on the plate surface, the convective heat transfer coefficient is typically compromised [1, 2]. Consequently, the design and optimization of SAHs become essential to enhance their efficiency and performance. A key aspect of SAH design entails the integration of rib-like structures onto the absorber plate, a strategy demonstrated to bolster heat transfer and fluid dynamics within the system. Although the addition of ribs to the absorber plate can effectively augment heat transfer, it also necessitates additional pumping energy due to the resulting pressure loss [3]. This trade-off between heat transfer enhancement and pressure loss has driven research aimed at optimizing the roughness features of the ribs. By meticulously designing the dimensions, shape, and arrangement of the ribs, previous work has sought to maximize heat transfer efficiency while mitigating the energy required for fluid circulation.

Numerous studies have investigated the flow characteristics and performance of SAHs with roughened absorber plates featuring ribs. Protruding wires, as first introduced by Prasad and Mullick [4], were found to enhance the heat transmission of SAHs, enabling quicker drying of wheat grains. Subsequent experimental research by Prasad and Saini [5] demonstrated that the height and pitch of ribs significantly improved flow

and heat transmission characteristics, leading to a 2.38-fold and 4.25-fold increase in the Nusselt number ( $Nu$ ) and friction factors, respectively. A variety of rib forms were tested by Karwa [6], including transverse, inclined, v-continuous, and v-discrete ribs in rectangular ducts. In another study, Layek et al. [7] evaluated the performance parameters of a SAH equipped with a transverse chamfered rib-groove turbulator. They reported maximum  $Nu$  at a chamfer angle of  $18^\circ$ , with friction increasing monotonously with the chamfer angle. Sivakumar et al. [8] conducted experimental research on the tendencies of  $Nu$  and friction loss within a rectangular convergent duct fitted with square ribs of varying sizes. They found that a rib height of 6 mm resulted in a threefold improvement in heat transfer compared to smooth counterparts.

While experimental assessment of SAH performance is both time-consuming and costly, computational fluid dynamics (CFD) has emerged as a valuable tool for analysing intricate fluid flow issues. Yadav and Bhagoria [9-12] utilised CFD to evaluate the performance of SAHs with rib-roughened absorber plates of various configurations. Their findings revealed higher thermal efficiency factors (TEFs) for operating Reynolds numbers ( $Re$ ) with  $P/e=10.71$  and  $e/D_h=0.04$ . However, their research was confined to specific rib geometries. Patel and Lanjewar [13] extended the numerical analysis of SAHs and identified a maximum TEF of 1.59 when a V-rib roughened SAH was used. Concurrently, Rasool and Qayoum [14] investigated the impact of ribs with different cross-sections on heat transfer and the friction factor in a two-pass square channel subjected to turbulent airflow. Their analysis revealed superior heat transfer and friction factor performance for designs incorporating boot-shaped ribs.

In addition, Ngo and Phu [15] conducted a computational analysis of SAHs with conic-curve profile ribs and reported a maximum TEF of 1.9 at  $Re=12,000$ . Mahanand and Senapati [16] discovered that at  $Re=15,000$ , SAH ducts with transverse inverted-T shaped ribs yielded the highest TEF of 1.86. In a subsequent numerical study, these authors examined the thermo-hydraulic features of a SAH with quarter-circular ribs and reported a maximum TEF of 1.88 [17].

A comprehensive review of the existing literature underscores the considerable importance of rib configuration and arrangement on the absorber plate for enhancing heat transfer in SAHs. Nonetheless, there is a noticeable research gap concerning the use of trapezoidal profile ribs as artificial roughness in SAH ducts. The geometric uniqueness of trapezoidal profile ribs, distinct from common rib shapes such as rectangular or circular, could induce specific flow patterns and heat transfer properties that remain largely unexplored. The primary objective of this study is to bridge this gap by conducting a rigorous investigation into the potential of trapezoidal profile ribs in SAHs and developing a numerical model to predict heat transfer and flow friction. Additionally, this study aims to determine the influence of relative rib pitch ( $P/e$ ) and height ( $e/D_h$ ) on average heat transfer and flow friction characteristics, with the goal of identifying the optimal rib configuration.

## 2. NUMERICAL ANALYSIS

### 2.1 Computational domain

Figure 1 depicts the 2\_D computation domain of a smooth SAH duct referred from Patel et al. [3]. The length of the SAH duct is divided into three portions, as per ASHRAE Standard 93 guidelines [18]: The entry portion ( $L_1=525$  mm), the test portion ( $L_2=1000$  mm), and the exit portion ( $L_3=875$  mm). The aspect ratio ( $W/H$ ) of the duct is maintained constant at 12 by making its height ( $H=25$  mm), its width ( $W=300$  mm), so the duct hydraulic diameter ( $D_h=46.1$  mm). In this study, a roughness element in the shape of transverse trapezoidal ribs (Figure 2) were fitted to the upper face of the bottom absorber plate. In situations involving rough surfaces or ribbed structures, the reattachment of the free shear layer is critical for successful heat transfer improvement. According to Verma and Prasad [19], the value of  $P/e$  cannot be less than 10. When the relative roughness pitch is sufficiently tiny ( $P/e < 10$ ), the roughness elements may prevent the divided shear layer from being reattached. Because of the altered flow patterns, this would result in a lack of effective heat transfer improvement and an increase in pressure drop [19]. As a result, maintaining an adequate  $p/e$  value is critical to ensuring that the roughness components or ribs do not interfere with flow reattachment and the resulting heat transfer increase. Therefore, three distinct values of rib-pitch ( $P=10, 15, 20$  mm) and rib-height ( $e=1, 1.5, 2$  mm) were chosen. The chosen range for rib height, between 1 mm and 2 mm, guarantees that the dimensions of the laminar sub-layer are comparable to the roughness height. This reduces the impact of the fins or the obstruction caused by the rib height on the flow characteristics of the system [9]. So, the relative roughness pitch ( $P/e$ ) varies between 5 and 20 (7 values), also the relative roughness height ( $e/D_h$ ) varies

between 0.021 and 0.043 (3 values). To assess the performance of SAH duct, seven Reynolds numbers ( $6,000 \leq Re \leq 18,000$ ) were chosen in turbulent flow regime.

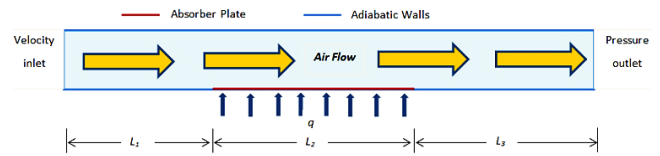


Figure 1. A sketch representing the computational domain

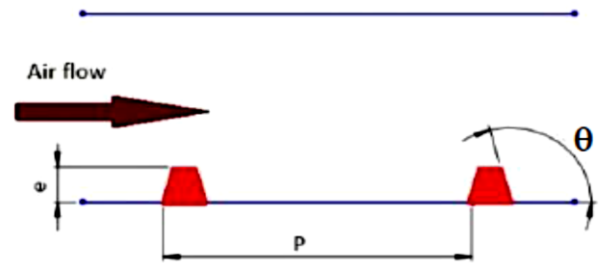


Figure 2. Configuration of roughness element

### 2.2 Assumption

The following assumptions simplify the flow field:

1. A steady, turbulent -fully developed flow.
2. Rib material, absorber plate, and duct wall are homogenous and isotropic.
3. SAH fluids and materials have constant thermal conductivity.
4. Air's thermo-physical properties are assumed constant at 300 K.
5. Neglecting radiation effect simplifies the heat transfer analysis, assuming that radiative heat transfer is minimal compared to convective heat transfer.

### 2.3 Grid generation

The mesh for the CFD analysis was generated using the meshing function offered by ANSYS. A non-uniform grid made of quadrilateral elements was developed, called an inflation grid, to efficiently capturing the higher gradients found close the wall, as depicted in Figure 3. A fine grid was used, with  $y^+ \approx 1$ , near the walls, where viscous effects have a pronounced impact on the flow behavior.

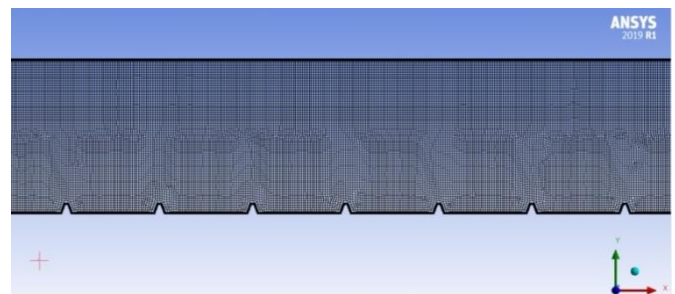


Figure 3. Grid layout of the domain with trapezoidal ribbed plate

## 2.4 Governing equations

This section summarizes the 2D- steady form of the continuity, momentum, and energy equation of turbulent flow within the SAH duct.

Continuity equation:

$$\frac{\partial(\rho u_i)}{\partial x_i} = 0 \quad (1)$$

Momentum equation:

$$\frac{\partial(\rho u_i u_j)}{\partial x_i} = -\frac{\partial p}{\partial x_i} + \frac{\partial}{\partial x_j} \left[ \mu \left( \frac{\partial(u_i)}{\partial x_j} + \frac{\partial(u_j)}{\partial x_i} \right) \right] + \frac{\partial(-\rho \bar{u}_i \bar{u}_j)}{\partial x_j} \quad (2)$$

Energy equation:

$$\frac{\partial}{\partial x_i} (\rho u_i T) = \frac{\partial}{\partial x_j} \left( (\Gamma + \Gamma_t) \frac{\partial T}{\partial x_j} \right) \quad (3)$$

where,  $\Gamma$  &  $\Gamma_t$  stand for, respectively, molecular and turbulent thermal diffusivities. They are denoted by the formulas below:

$$\Gamma = \frac{\mu}{Pr} \quad (4)$$

$$\Gamma_t = \frac{\mu_t}{Pr_t} \quad (5)$$

The Reynolds number is given as:

$$Re = \frac{\rho v D_h}{\mu} \quad (6)$$

For roughened SAH, the average  $Nu$  and  $f$  are defined respectively as:

$$\overline{Nu_r} = \frac{h D_h}{k} \quad (7)$$

$$\bar{f}_r = \frac{(\Delta P / l) D_h}{2 \rho v^2} \quad (8)$$

To study the total performance, both the thermal and hydraulic properties of the SAH should be considered. Webb and Eckert [20] introduced an indicator for comparing the heat transfer performance of a modified duct, such as one with roughened surfaces, to that of a smooth one under the condition of constant pumping power. This performance indicator is known as the thermo-hydraulic performance factor (TPF).

$$TPF = \frac{Nu_r / Nu_s}{\left( \bar{f}_r / \bar{f}_s \right)^{1/3}} \quad (9)$$

$Nu_s$ ,  $f_s$  in Eq. (9) represent Nusselt number and friction factor for smooth SAH duct. They can be estimated with the

Dittus Boelter equation [21], and modified Blasius equation [22] respectively as per Eqs. (10) and (11).

$$Nu_s = 0.023 Re^{0.8} Pr^{0.4} \quad (10)$$

$$f_s = 0.085 Re^{-0.25} x_{1,2} = \frac{-b \pm \sqrt{b^2 - 4ac}}{2a} \quad (11)$$

## 2.5 Selection of turbulence model

Yadav and Bhagoria [10, 12] examined five different turbulence models, including the Standard  $k$ - $\epsilon$ , RNG  $k$ - $\epsilon$ , Realizable  $k$ - $\epsilon$ , Standard  $k$ - $\epsilon$ , and SST  $k$ - $\epsilon$ , to simulate the flow through the SAH. They found that the RNG  $k$ - $\epsilon$  model was the best one when compared the predicted data with the available experimental data. Thus, for the current investigation, the RNG  $k$ - $\epsilon$  turbulence model was used to estimate the flow and heat transmission characteristics within an artificially roughened SAH.

The transport equations for predicting the turbulent kinetic energy,  $k$ , and its rate of dissipation,  $\epsilon$ , are as follows:

$$\frac{\partial(\rho k u_i)}{\partial x_i} = \frac{\partial}{\partial x_j} \left( \alpha_k \mu_{eff} \frac{\partial k}{\partial x_j} \right) + G_k - \rho \epsilon \quad (12)$$

$$\frac{\partial(\rho \epsilon u_i)}{\partial x_i} = \frac{\partial}{\partial x_j} \left( \alpha_\epsilon \mu_{eff} \frac{\partial \epsilon}{\partial x_j} \right) + C_{1\epsilon} \frac{\epsilon}{k} (G_k) - C_{2\epsilon} \rho \frac{\epsilon^2}{k} - R_\epsilon \quad (13)$$

$\alpha_k$  &  $\alpha_\epsilon$  are known as "inverse-turbulent Prandtl numbers". Also,

$$\mu_{eff} = \mu + \mu_t \quad (14)$$

$$\mu_t = \rho C_\mu \frac{k^2}{\epsilon} \quad (15)$$

$$G_k = -\rho \bar{u}_i \bar{u}_j \frac{\partial u_j}{\partial x_i} \quad (16)$$

where,  $C_{1\epsilon}$ ,  $C_{2\epsilon}$ ,  $C_\mu$ ,  $\alpha_k$  and  $\alpha_\epsilon$  are the model constants possessing the subsequent default values [23]:

$$C_{1\epsilon}=1.42, C_{2\epsilon}=1.68, C_\mu=0.0845, \alpha_k=1.39, \alpha_\epsilon=1.39.$$

## 2.6 Boundary condition

In modeling and simulating solar air heaters, boundary conditions are crucial. These factors should be carefully considered by researchers to guarantee that the results are significant and applicable to specific real-world settings. Ignoring or oversimplifying boundary criteria might severely limit the validity and practical significance of the investigation.

In this study, a consistent air velocity and temperature were imposed at the inlet, whereas the output has a pressure outlet condition with a fixed pressure of 1.013e5 Pa. The duct walls are non-slip and impermeable. The absorber plate gets a 1000 W/m<sup>2</sup> uniform flux, while the bottom wall stays adiabatic. The inlet velocity values are calculated using Re, which has seven separate values ranging from 1.9 m/s to 5.7 m/s, equating to a Re of 6,000-18,000.

## 2.7 Solution method

The governing equations were solved via FVM approach in ANSYS - Fluent version 2019 R1. When capturing flow gradients and variations, second-order upwind-biased discretization is frequently recommended. Therefore, the equations were discretized using a second-order upwind-biased, then solved via pressure-based solver in ANSYS - Fluent. Proper pressure-velocity coupling is critical in SAH simulations for accurate predictions of flow patterns and heat transfer. Therefore, the SIMPLE algorithm was used since it successfully manages the iterative coupling of pressure and velocity fields. For spatial discretization, the least square cell approach was employed. Convergence criteria were set based on residuals to ensure solution accuracy. The convergence criterion should be properly calibrated in order to balance computational resources and solution correctness, resulting in dependable results. So, a residual threshold of  $10^{-4}$  was used for the continuity and momentum equations, while a more stringent threshold of  $10^{-8}$  was used for the energy equation.

To compute the heat transfer coefficient ( $h$ ) and the pressure drop across the test section, surface integrals within ANSYS - Fluent were utilized. These integrals provide a means to calculate the average values of  $Nu$  (Eq. (7)) and the friction factor (Eq. (8)).

## 3. RESULTS AND DISCUSSION

### 3.1 Grid independence test

To ensure the reliability and dependability of the simulation results, a grid-independence test (GIT) was conducted employing five different sets of grids with varying sizes. Specifically, the GIT was performed on a trapezoidal ribbed SAH with  $e/D_h=0.032$  and  $Re=12,000$ . The GIT indicates that for the specific case considered, when the number of cells exceeds 427,772, the  $Nu$  and friction factor ( $f$ ) values exhibit negligible changes with relative variations of 0.147% and 0.2019%, respectively. Based on this observation, it is concluded that using 427,772 cells provides a sufficient grid density for accurate results in this case.

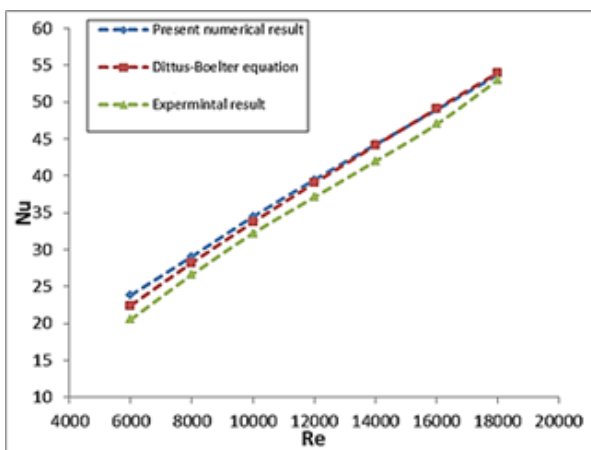
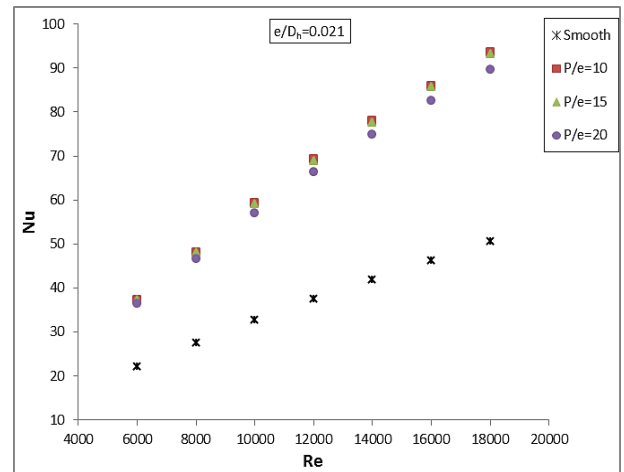


Figure 4. Comparison of the present  $Nu$  numerical finding with empirical correlations and experimental data

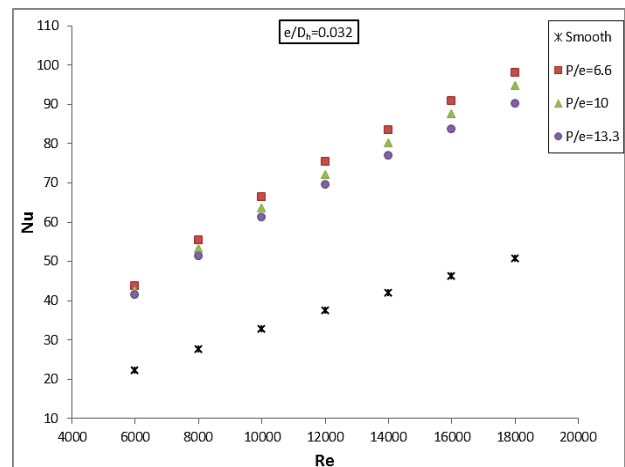
### 3.2 Validation of CFD model

The  $Nu$  for the smooth duct estimated using the current

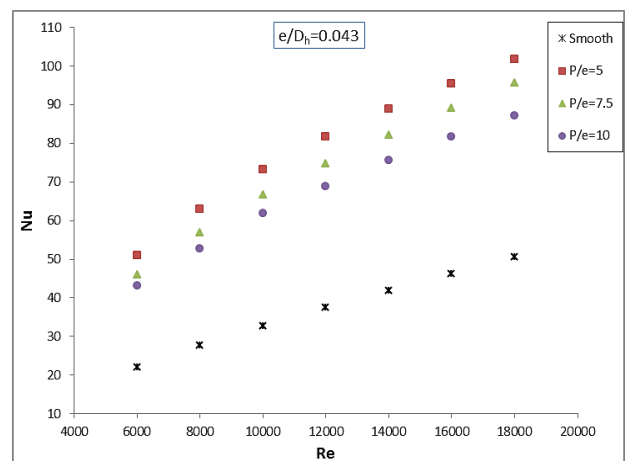
numerical approach were compared to those derived using Eq. (10). Moreover, the numerical results were also compared with experimental data of Patel et al. [3]. Figure 4 depicts a comparison of present numerical findings for the smooth duct with empirical correlation and experimental data. It is obvious that the  $Nu$  plot always exhibit the same patterns with maximum deviation from the empirical correlation was determined to be 6%, while the variation with the experimental data ranged from 1.28 to 8.4%. Based on this comparison, it can be concluded that the current numerical technique provides acceptable results.



(a)



(b)



(c)

Figure 5. Variation of  $Nu$  versus  $Re$  for varied  $e/D_h$  and  $P/e$  values

### 3.3 Heat transfer features

Figure 5 depicts a plot of  $Nu$  versus  $Re$  for varied  $e/D_h$  and  $P/e$  values. It can be seen the presence of ribs clearly improves the average  $Nu$  as compared to a smooth duct. It was discovered that the  $Nu$  grows inexorably with an increase in  $Re$ . It is generally understood that increasing the  $Re$  boosts the turbulent kinetic energy and turbulent dissipation rate, which eventually results in an upsurge in turbulent intensity and hence the  $Nu$ . Additionally, as  $Re$  grows, the boundary layer's thickness reduces which improving overall heat transmission. A vortex formed near the top surface of the rib due to the increased turbulence brought on by the velocity increase, which helped to improve heat transmission from the heated plate to the surrounding air. Additionally, the presence of ribs also contributes to local heat removal through the generation of vortices. These vortices create additional turbulence and enhance the heat transfer at the local level. The vortices promote better mixing of the fluid, leading to increased heat transfer rates and improved thermal performance of the system. This local contribution further enhances the overall heat removal capability of the roughened surface in comparison to a smooth surface. At  $e/D_h=0.043$ ,  $P/e=5$  and  $Re=6,000$ , it was discovered that the highest enhancement of average  $Nu$  was 2.314 times that of smooth duct. Table 1 illustrates the enhancement ratio of the average  $Nu$  for a variety of  $e/D_h$  and  $P/e$  values.

From Figure 5 two additional trends can be clearly seen. The first trend; the average  $Nu$  increases with  $e/D_h$ . This trend confirms the positive influence of higher rib heights on heat transmission. This behavior is a result of the increased reconnecting of the free shear layer generated by roughness elements. When the relative roughness height is higher, it creates more disruptions in the flow, leading to the formation of stronger secondary flows and vortices. These secondary flows contribute to better heat transfer by enhancing fluid mixing and promoting the exchange of heat between the heated surface and the surrounding fluid. The findings indicate that the maximal  $Nu$  value was achieved at  $e/D_h=0.043$  for the investigated range of parameters.

The second trend; the average  $Nu$  number falls as  $P/e$  rises. This is because the number of reattachment locations over the absorber plate decreases with increasing relative roughness pitch.

The heat transfer features in a roughened SAH can be effectively illustrated and explained through the use of contour plots depicting the distribution of turbulent kinetic energy (TKE) and turbulent intensity (TI). The comparison of TKE and TI contours at different  $Re$  values has been displayed in Figure 6 and Figure 7. Turbulent kinetic energy represents the energy associated with the turbulent motion of the fluid.

Contour plots of turbulent kinetic energy provide valuable insights into the intensity and distribution of turbulence within the SAH duct. Areas with higher values of turbulent kinetic energy indicate regions of increased turbulence and enhanced heat transfer.

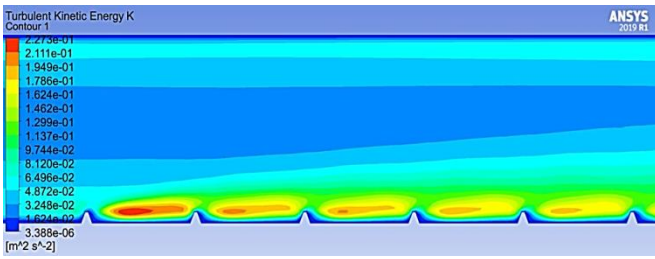
It is noticeable from Figure 6 and Figure 7, that the presence of ribs increases the TKE and TI close to the rib zone. Large amounts of TKE are predicted at the first rib pair, leading to a significant impact of turbulent intensity on heat transfer enhancement at this location. Following the first pair of ribs in the same direction as the flow, the levels of both of the turbulence parameters (TKE and TI) then begin to fall. The greater the value of the turbulence parameters, the more intense the turbulence in the specified region; consequently, the shear stress is also more intense there. The flow is developing close to the entrance, shear stress is predominating within the boundary layer. Therefore, the highest levels of turbulence and kinetic energy are found in the region of the first ribs. As the flow progressed from the inlet to the outlet, it become fully developed and lost some of its kinetic energy and turbulence. Also, as a result of the collision of high-fluid velocity on those surfaces (Ribs), eddies would form more frequently in the area close to the ribs this also adds to an increase in the value of both the turbulence parameters. The high wall shear and the subsequent creation of vortices between the ribs and the absorber plate promote rapid diffusion into the main flow, thereby increasing heat transmission from the plate. The contours plots of Figure 6 and Figure 7. also indicate that as the  $Re$  grows, so does the quantity of turbulence, resulting in increased values of turbulent parameters.

Finally, by examining these contour plots, one can identify the regions within the SAH duct where the TKE and TI are maximized. These regions typically coincide with the presence of roughness elements, such as ribs, on the absorber plate. The roughness elements disrupt the flow and generate turbulence, leading to improved heat transmission. Furthermore, the contour plots help to visualize the flow patterns and identify areas of recirculation and flow separation, which are associated with increased turbulence and heat transfer enhancement. The formation of vortices and the interaction of the fluid with the roughness elements can be observed, providing a comprehensive understanding of the flow dynamics and heat transfer mechanisms.

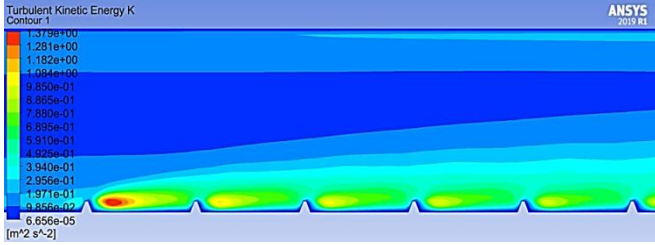
The velocity contours plot of the proposed rib form are shown in Figure 8 with a constant value of  $Re$  of 18,000,  $P/e=10$ , and varied  $e/D_h$  values. The presence of ribs on the surface of absorber plate introduces irregularities in the flow patterns, causing the development of eddies near the ribs. This can be observed by examining the instantaneous velocity contours.

**Table 1.**  $Nu$  augmentation ratio ( $Nu_r/Nu_s$ ) at different  $e/D_h$  and  $P/e$  values

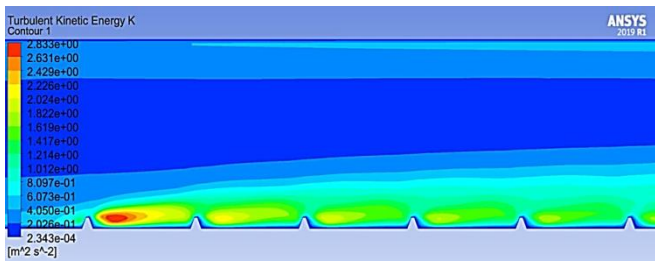
$e/D_h$	$P/e$	$Re=6,000$	$Re=8,000$	$Re=10,000$	$Re=12,000$	$Re=14,000$	$Re=16,000$	$Re=18,000$
0.021	10	1.682	1.744	1.815	1.847	1.858	1.857	1.851
	15	1.684	1.742	1.808	1.840	1.850	1.849	1.841
	20	1.652	1.691	1.746	1.774	1.784	1.782	1.772
0.032	6.6	1.978	2.008	2.029	2.016	1.990	1.964	1.937
	10	1.915	1.923	1.940	1.925	1.908	1.888	1.870
	13.3	1.876	1.864	1.872	1.858	1.833	1.809	1.785
0.043	5	2.314	2.285	2.242	2.180	2.118	2.062	2.011
	7.5	2.081	2.058	2.037	1.998	1.959	1.925	1.893
	10	1.959	1.914	1.892	1.841	1.805	1.767	1.723



(a)

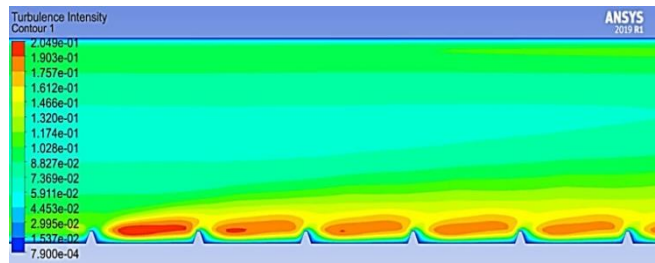


(b)

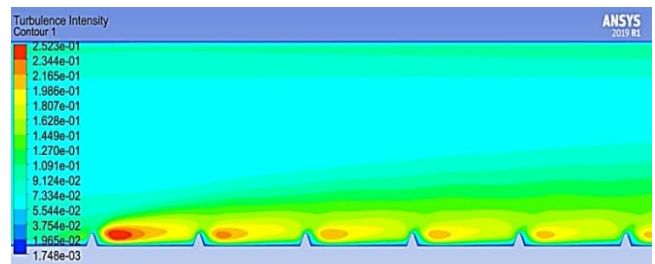


(c)

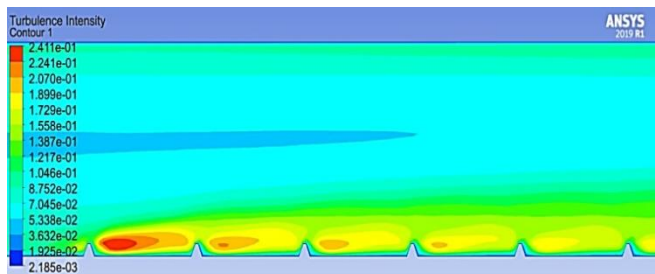
**Figure 6.** Contours of TKE for  $P/e=10$  and  $e/D_h=0.032$  at (a)  $Re=6,000$ , (b)  $Re=12,000$ , (c)  $Re=18,000$



(a)



(b)

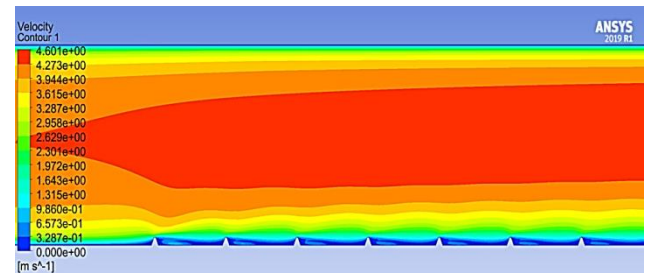


(c)

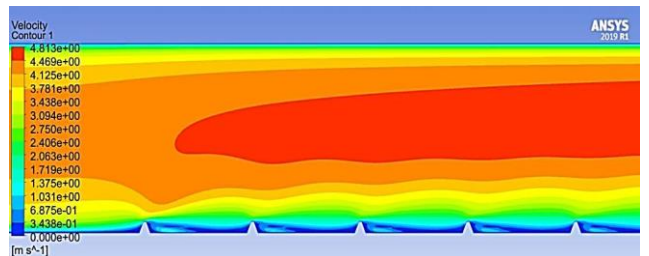
**Figure 7.** Contours of TI for  $P/e=10$  and  $e/D_h=0.032$  at (a)  $Re=6,000$ , (b)  $Re=12,000$ , (c)  $Re=18,000$

The irregularity in the velocity contours arises from the interaction between the fluid flow and the roughness elements. The ribs create disruptions and obstacles in the flow, causing the fluid to change direction and form vortices. These vortices, or eddies, are characterized by swirling motions and localized regions of higher and lower velocities. The development of eddies is advantageous for enhancing heat transmission. The eddies improve fluid mixing, which in turn increases fluid contact with the heated surface. This enhanced mixing facilitates the transfer of heat from the surface to the fluid, resulting in improved heat transfer performance.

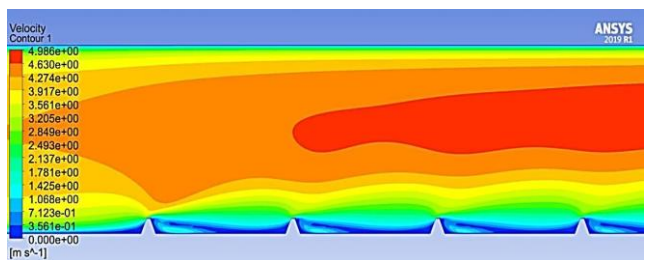
It is seen that the velocity increases along the roughened duct of SAH, which is a result of the ribs placed on the absorber plate acting as nozzles that accelerate the fluid flow locally. As the fluid velocity increases suddenly, a separation zone forms downstream of the rib; the flow then reattaches in the leading edge of the succeeding rib. A second, smaller eddy is formed due to the continual reattaching and recirculating of flow impacted by the main stream and impinging on the wall. Fluid flow is really deflected by the presence of roughened components, as stated by Chandra et al. [24], and reattaches 5-6 times  $e/D_h$  further downstream.



(a)



(b)



(c)

**Figure 8.** Velocity contours at  $Re=12,000$ ,  $P/e=10$  and (a)  $e/D_h=0.021$  at, (b)  $e/D_h=0.032$ , (c)  $e/D_h=0.043$

### 3.4 Friction factor features

The plots of friction factor vs  $Re$  at varying  $P/e$  and  $e/D_h$  values are shown in Figure 9 (a)-(c). It is self-evident that roughness elements enhance the average friction factor in comparison to a smooth duct. As might be predicted from the findings, the average  $f$  decreases as  $Re$  increases. It is

commonly known that when the  $Re$  increases, the flow velocity rises and the boundary layer thins, so the viscous sub-layer is also dampened, resulting in reduced average  $f$  values. Additionally, it was shown that the friction factor rose with an increase in  $e/D_h$  at a specific value of  $Re$  and  $P/e$ , which is due to an increase in flow obstruction with increasing  $e/D_h$ . Table 2 summarizes the friction enhancement factor ( $f_r/f_s$ ) for various  $P/e$  and  $e/D_h$  values. The highest increment in the average  $f$  was determined to be 3.425 times greater than that of a smooth duct at  $e/D_h=0.043$ ,  $P/e=5$  and  $Re$  of 16,000.

Furthermore, it is evident from Figure 9 that the friction factor increases as  $e/D_h$  increases, this is due to increased flow interruptions within the ribbed SAH duct. Also, for a given value of  $e/D_h$ , it has been shown that as  $P/e$  increases, the number of breaks in the flow path decreases, therefore the average friction factor drops. Low flow resistance is achieved via the SAH duct, which features fewer trapezoidal sectioned ribs at higher pitch.

### 3.5 Thermo-hydraulic performance features

By continuously separating and reattaching the flow stream,

artificial roughness reduces thermal resistance, increases heat transfer, and disrupts the laminar sub-layer. The increased heat transmission is, unfortunately, dismissed out by the increased pumping power required due to fluid friction. As a result, the efficiency and effectiveness of a roughened SAH to increase heat transmission with minimal pumping power are held in high esteem. The CFD study reveals roughened SAH with  $e/D_h=0.043$ ,  $P/e=5$  and at  $Re=6,000$  achieves a maximum  $Nu$  enhancement ratio of 2.314 and a greatest friction factor of 3.425 times that of smooth ducts at  $Re=16,000$ . Therefore, assessing the efficacy of a ribbed SAH requires considering both thermal and hydraulic performances. Webb and Eckert [20] introduced the thermo-hydraulic performance factor (TPF) in Eq. (9). This indicator evaluates system efficiency by comparing heat transfer enhancement to pressure drop or pumping power increment. Figure 10 displays the plot of TPF versus  $Re$  at different  $e/D_h$  and  $P/e$  values. It was shown that the variance of TPF in ranges from 1.172 to 1.41. According to the investigated parameter range, the absorber plate with trapezoidal ribs has the highest TPF of 1.64 at a  $Re=6,000$ ,  $e/D_h=0.043$  and  $P/e=5$ .

**Table 2.** Friction increment ratio ( $f_r/f_s$ ) at different  $e/D_h$  and  $P/e$  values

$e/D_h$	$P/e$	$Re=6,000$	$Re=8,000$	$Re=10,000$	$Re=12,000$	$Re=14,000$	$Re=16,000$	$Re=18,000$
0.021	10	1.646	1.773	1.895	1.988	2.062	2.095	2.099
	15	1.511	1.620	1.744	1.821	1.899	1.938	1.972
	20	1.427	1.531	1.645	1.724	1.792	1.836	1.886
0.032	6.6	2.312	2.462	2.654	2.743	2.827	2.895	2.913
	10	2.172	2.314	2.490	2.573	2.683	2.706	2.721
	13.3	2.067	2.211	2.370	2.463	2.571	2.597	2.611
0.043	5	2.818	3.121	3.317	3.395	3.423	3.425	3.415
	7.5	2.755	3.022	3.203	3.259	3.270	3.268	3.261
	10	2.675	2.925	3.160	3.178	3.183	3.180	3.180

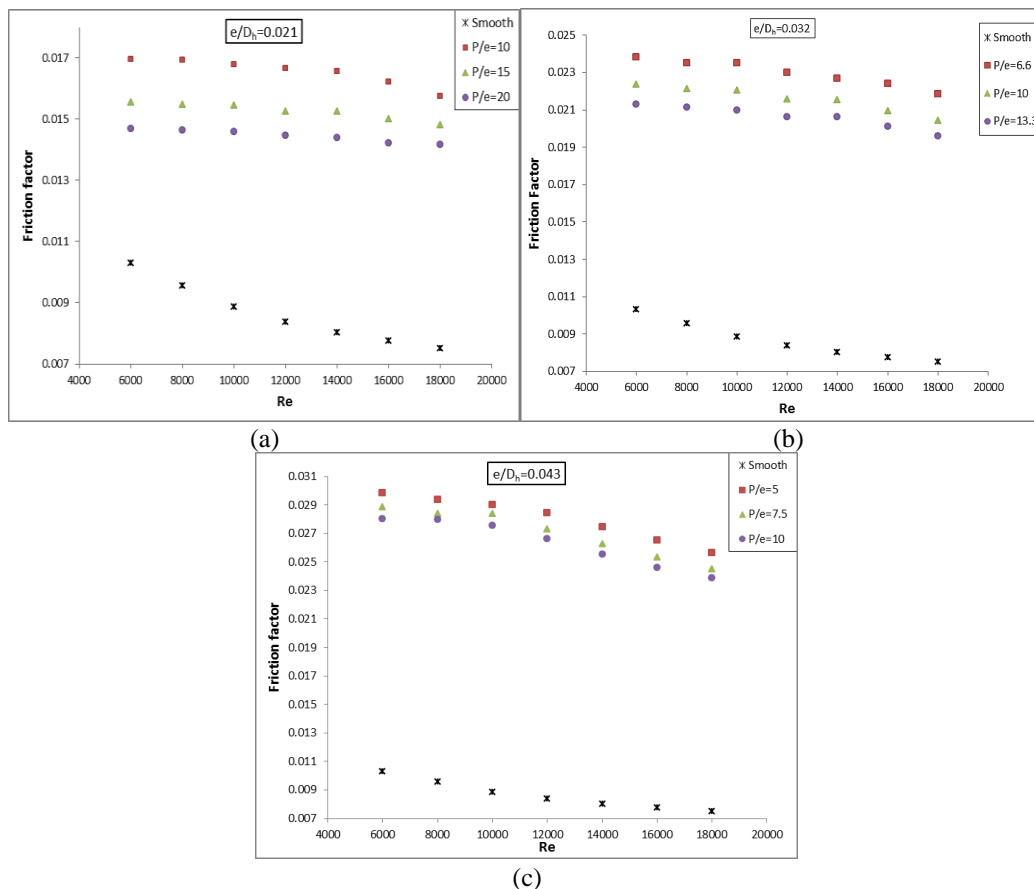


**Figure 9.** Variation of friction factor versus  $Re$  for varied  $e/D_h$  and  $P/e$  values

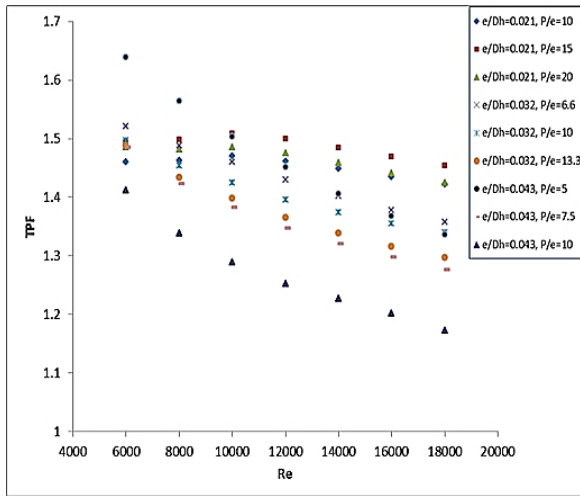


**Figure 10.** Variation of TPF with  $Re$  for different  $e/D_h$  and  $P/e$  values

#### 4. CONCLUSIONS

The 2-D turbulent air flow and heat transmission characteristics within a rectangular duct of a SAH with one roughened wall and transverse-trapezoidal ribs are analyzed numerically. The properties of heat transmission, flow friction, and flow structure are described and analyzed. The primary findings of this study are:

- Utilizing artificial irregularities on an absorber plate's surface is an excellent method for increasing the rate of heat transmission.
- The  $Nu$  rises while the friction factor falls as the Reynolds number increases. When compared to a smooth absorber plate, the friction factor and  $Nu$  are larger. This is due to a change in flow characteristics caused by roughness, which generates flow separation, reattachments, and secondary flow generation.
- The  $Nu$  of roughened SAH increases with both  $Re$  and  $e/D_h$  for a fixed ratio of  $P/e$ . However, as  $Re$  increases and  $e/D_h$  decreases, the friction factor falls.
- At  $e/D_h=0.043$ ,  $p/e=5$  and  $Re=6,000$ , the largest  $Nu$  enhancement ratio was found to be as much as 2.124 times higher than that of the smooth duct. Whereas, the maximum friction factor increment ratio was found to be 3.425 at  $Re=16,000$ .
- TPF for SAH with trapezoidal ribs at  $e/D_h=0.043$ ,  $p/e=5$  reaches its maximum value of 1.64 at  $Re=6,000$ .

An outcome, it is recommended to use a solar air heater with artificial roughening, specifically with trapezoidal-sectioned transverse rib roughness on the absorber plate, where the rib pitch to rib height ( $P/e$ ) ratio is 10.71 and the rib height to hydraulic diameter ( $e/D_h$ ) ratio is 0.043. This arrangement has been shown to improve heat transfer in such systems. However, there is a scarcity of research utilizing trapezoidal-sectioned ribs with different slope to investigate the impact of rib tip angle variations on roughened SAH performance.

#### REFERENCES

[1] Kumar, S., Das, R.K., Kulkarni, K. (2022). Comparative study of solar air heater (SAH) roughened with

transverse ribs of NACA 0020 in forward and reverse direction. *Case Studies in Thermal Engineering*, 34: 102015. <https://doi.org/10.1016/j.csite.2022.102015>

[2] Patel, Y.M., Jain, S.V., Lakhera, V.J. (2021). Thermo-hydraulic performance analysis of a solar air heater roughened with discrete reverse NACA profile ribs. *International Journal of Thermal Sciences*, 167: 107026. <https://doi.org/10.1016/j.ijthermalsci.2021.107026>

[3] Patel, Y.M., Jain, S.V., Lakhera, V.J. (2020). Thermo-hydraulic performance analysis of a solar air heater roughened with reverse NACA profile ribs. *Applied Thermal Engineering*, 170: 114940. <https://doi.org/10.1016/j.applthermaleng.2020.114940>

[4] Prasad, K., Mullick, S. (1983). Heat transfer characteristics of a solar air heater used for drying purposes. *Applied Energy*, 13(2): 83-93. [https://doi.org/10.1016/0306-2619\(83\)90001-6](https://doi.org/10.1016/0306-2619(83)90001-6)

[5] Prasad, B., Saini, J. (1988). Effect of artificial roughness on heat transfer and friction factor in a solar air heater. *Solar Energy*, 41(6): 555-560. [https://doi.org/10.1016/0038-092X\(88\)90058-8](https://doi.org/10.1016/0038-092X(88)90058-8)

[6] Karwa, R. (2003). Experimental studies of augmented heat transfer and friction in asymmetrically heated rectangular ducts with ribs on the heated wall in transverse, inclined, V-continuous and V-discrete pattern. *International Communications in Heat and Mass Transfer*, 30(2): 241-250. [https://doi.org/10.1016/S0735-1933\(03\)00035-6](https://doi.org/10.1016/S0735-1933(03)00035-6)

[7] Layek, A., Saini, J., Solanki, S. (2009). Effect of chamfering on heat transfer and friction characteristics of solar air heater having absorber plate roughened with compound turbulators. *Renewable Energy*, 34(5): 1292-1298. <https://doi.org/10.1016/j.renene.2008.09.016>

[8] Sivakumar, K., Natarajan, E., Kulasekharan, N. (2014). Experimental studies on turbulent flow in ribbed rectangular convergent ducts with different rib sizes. *International Journal of Heat and Technology*, 32(1&2): p. 79-85. <https://doi.org/10.18280/ijht.320112>

[9] Yadav, A.S., Bhagoria, J. (2014). A numerical investigation of square sectioned transverse rib roughened solar air heater. *International Journal of Thermal Sciences*, 79: 111-131. <https://doi.org/10.1016/j.ijthermalsci.2014.01.008>

[10] Yadav, A.S., Bhagoria, J. (2013). A CFD based heat transfer and fluid flow analysis of a solar air heater provided with circular transverse wire rib roughness on the absorber plate. *Energy*, 55: 1127-1142. <https://doi.org/10.1016/j.energy.2013.03.066>

[11] Yadav, A.S., Bhagoria, J. (2014). A numerical investigation of turbulent flows through an artificially roughened solar air heater. *Numerical Heat Transfer, Part A: Applications*, 65(7): 679-698. <https://doi.org/10.1080/10407782.2013.846187>

[12] Yadav, A.S., Bhagoria, J. (2014). A CFD based thermo-hydraulic performance analysis of an artificially roughened solar air heater having equilateral triangular sectioned rib roughness on the absorber plate. *International Journal of Heat and Mass Transfer*, 70: 1016-1039. <https://doi.org/10.1016/j.ijheatmasstransfer.2013.11.074>

[13] Patel, S.S., Lanjewar, A. (2019). Experimental and numerical investigation of solar air heater with novel V-rib geometry. *Journal of Energy Storage*, 21: 750-764. <https://doi.org/10.1016/j.est.2019.01.016>

- [14] Rasool, A., Qayoum, A. (2018). Numerical analysis of heat transfer and friction factor in two-pass channels with variable rib shapes. *International Journal of Heat & Technology*, 36(1): 40-48. <https://doi.org/10.18280/ijht.360106>
- [15] Ngo, T.T., Phu, N.M. (2020). Computational fluid dynamics analysis of the heat transfer and pressure drop of solar air heater with conic-curve profile ribs. *Journal of Thermal Analysis and Calorimetry*, 139: 3235-3246. <https://doi.org/10.1007/s10973-019-08709-4>
- [16] Mahanand, Y., Senapati, J.R. (2020). Thermal enhancement study of a transverse inverted-T shaped ribbed solar air heater. *International Communications in Heat and Mass Transfer*, 119: 104922. <https://doi.org/10.1016/j.icheatmasstransfer.2020.104922>
- [17] Mahanand, Y., Senapati, J.R. (2021). Thermo-hydraulic performance analysis of a solar air heater (SAH) with quarter-circular ribs on the absorber plate: A comparative study. *International Journal of Thermal Sciences*, 161: 106747. <https://doi.org/10.1016/j.ijthermalsci.2020.106747>
- [18] Handbook, A.A., Atlanta, G. (2003). UAS: American Society of Heating, Refrigerating and Air Conditioning Engineers.
- [19] Verma, S.K., Prasad, B.N. (2000). Investigation for the optimal thermohydraulic performance of artificially roughened solar air heaters. *Renewable Energy*, 20(1): 19-36. [https://doi.org/10.1016/S0960-1481\(99\)00081-6](https://doi.org/10.1016/S0960-1481(99)00081-6)
- [20] Webb, R., Eckert, E. (1972). Application of rough surfaces to heat exchanger design. *International Journal of Heat and Mass Transfer*, 15(9): 1647-1658. [https://doi.org/10.1016/0017-9310\(72\)90095-6](https://doi.org/10.1016/0017-9310(72)90095-6)
- [21] McAdams, W. (1954). *Heat Transfer*. McGraw-Hill, New York, 3.
- [22] Fox, R.W., McDonald, A.T., Pritchard, P.J. (1994). *Introduction to Fluid Mechanics*. John Wiley & Sons, Inc., New York.
- [23] Launder, B.E., Spalding, D.B. (1972). *Lectures in Mathematical Models of Turbulence*. Academic Press, London, New York.
- [24] Chandra, P.R., Fontenot, M.L., Han, J.C. (1998). Effect of rib profiles on turbulent channel flow heat transfer. *Journal of Thermophysics and Heat Transfer*, 12(1): 116-118. <https://doi.org/10.2514/2.6312>

## NOMENCLATURE

$D_h$	Hydraulic diameter, m
$e/D_h$	Relative roughness height
$P/e$	Relative roughness pitch
$H$	Depth of duct, m
$W$	Width of duct, m
$Nu$	Nusselt number
$f$	Friction factor
$Re$	Reynolds number

## Greek symbols

$\rho$	Density, $\text{kg/m}^3$
$\mu$	Dynamic viscosity, $\text{kg} \cdot \text{m}^{-1} \cdot \text{s}^{-1}$

## Subscripts

s	Smooth duct
r	Roughened duct